

Improved Estimation Accuracy in OFDM-based Joint Communication and Sensing through Kalman Tracking and Interpolation

Charlotte Muth, Leon Schmidt, Shrinivas Chimmalg, and Laurent Schmalen
Communications Engineering Lab (CEL), Karlsruhe Institute of Technology (KIT)
Hertzstr. 16, 76187 Karlsruhe, Germany, Email: muth@kit.edu

Abstract—We investigate a monostatic orthogonal frequency-division multiplexing (OFDM)-based joint communication and sensing (JCAS) system for object tracking. Our setup consists of a transmitter and receiver equipped with an antenna array for fully digital beamforming. The native resolution of all radar-like sensing, including OFDM radar sensing, is limited by the observation time and bandwidth. In this work, we improve the parameter estimates through interpolation methods and tracking algorithms. We verify our method by comparing the root mean squared error (RMSE) of the estimated range, velocity and angle and by comparing the mean Euclidean distance between the estimated and true position. We demonstrate how both a Kalman filter for tracking, and interpolation methods using zero-padding and the chirp Z-transform (CZT) improve the estimation error. We discuss the computational complexity of the different methods. We propose the KalmanCZT approach that combines tracking via Kalman filtering and interpolation via the CZT, resulting in a solution with flexible resolution that significantly improves the range RMSE.

Index Terms—Joint Communication and Sensing, OFDM, Tracking, Kalman Filter, Interpolation

I. INTRODUCTION

Joint communication and sensing (JCAS) is a technology to be integrated into the new 6G standard [1] that adds a sensor functionality to wireless communication devices. Different features of the environment can be sensed as transmit signals are reflected by passive objects resulting in multiple reflections of the same signal being received. These reflections can be identified and attributed to different objects in the environment, transforming devices for wireless communication into potential sensors. Different applications have been proposed including weather monitoring, network optimization, traffic assistance or drone detection. Additionally, an improvement in energy and spectral efficiency is expected compared to deploying separate radar and communication systems.

Orthogonal frequency-division multiplexing (OFDM) is especially suitable as a waveform for 6G JCAS as it is a well established waveform for communication, as it enables robust communication in frequency-selective channels for low computational resources. Additionally, it has been studied for

application in radar for over a decade [2]. However, precise radar estimates rely on sufficient observation time and a large signal bandwidth. Bandwidth remains a finite resource as different systems operate simultaneously and interference has to be prevented. In 6G, we expect a limited bandwidth that is primarily chosen for communication, limiting the sensing resolution. In particular, the limited range resolution contributes severely to the estimation error when localizing objects that do not communicate.

If we want to capture a trajectory in time, limited resolution makes a single estimate inaccurate. Methods such as tracking and interpolation offer more accurate estimates of the spatial environment. A well-designed interpolation approach improves the ability of the system to distinguish between closely spaced objects and increases the estimation precision, effectively increasing the detail of the sensed environment. Interpolation approaches for sensing include zero-padding (ZP), the chirp Z-transform (CZT) [3], or super-resolution methods [4]. Tracking additionally helps to maintain consistent observations of moving targets, allowing for the prediction of their future positions, which is vital for navigation, collision avoidance, and beamforming. If positions follow a trajectory, we can use prediction to refine the estimates, as the positions along a trajectory are typically correlated. Numerous studies applying Kalman filters to object tracking are part of the radar literature, e.g. in FMCW radar [5]. Especially, angle of arrival tracking has been of interest, since it enables precise beam tracking [6]. True position tracking can potentially further enhance energy-aware beam tracking. Additionally, object tracking is a basic task for OFDM-based JCAS systems and therefore of interest [7] in order to track, e.g., obstacles in traffic or drones. In order to enable real-time tracking, the complexity of the resolution enhancement algorithm needs to be sufficiently low, yet it should yield a position estimate that is as accurate as possible.

This paper specifically compares Kalman filtering structures and interpolation methods to improve tracking estimation in an OFDM-based JCAS system. We discuss how the computational complexity can be limited and how the estimation results are affected by interpolation and tracking, respectively. We present an alternative event-based measurement approach and propose the KalmanCZT as a combination approach of interpolation and tracking.

This work has received funding in part from the European Research Council (ERC) under the European Union's Horizon 2020 research and innovation programme (grant agreement No. 101001899) and in part from the German Federal Ministry of Education and Research (BMBF) within the projects Open6GHub (grant agreement 16KISK010) and KOMSENS-6G (grant agreement 16KISK123).

II. SYSTEM MODEL

In this paper, we investigate a monostatic OFDM-based JCAS setup, where the transmitter and the sensing receiver are co-located, i.e., part of the same base station, and are equipped with uniform linear arrays (ULAs) to perform digital beamforming. Our goal is to track the angle of arrival (AoA), range and radial velocity of a passive object based on its reflection to track its location in a 2D plane. The transmit signal is simultaneously used to communicate with a user equipment (UE) equipped with a single antenna in a *separate* area of interest. We simulate a split transmit beam to enable communication, yet focus on the object tracking in this work. This approach enables us to use samples beyond the pilots for sensing which increases the accuracy for sensing.

A. Transmitter

We consider an OFDM signal with N orthogonal sub-carriers with sub-carrier spacing $\Delta f = B/N = 1/(T_s N) = 1/T$, bandwidth B , sample duration T_s , and OFDM symbol duration T . M OFDM symbol vectors are processed together in an OFDM frame. The NM transmit symbols of a frame are selected from the QPSK modulation alphabet and can be arranged as a matrix \mathbf{X} of dimension $N \times M$. The notation $\mathbf{X}[n, m]$ denotes the element of \mathbf{X} in the n th row and m th column, corresponding to the symbol of the n th sub-carrier of the m th OFDM symbol in a frame. A cyclic prefix (CP) of duration T_{cp} is added to each symbol before transmitting the equivalent baseband signal [2]

$$s(t) = \frac{1}{\sqrt{N}} \sum_{m=0}^{M-1} \sum_{n=0}^{N-1} \mathbf{X}[n, m] e^{j2\pi n \Delta f (t - mT_0)} g(t - mT_0),$$

where $T_0 = T_{cp} + T$ and $g(t) = 1$ for $t \in [-T_{cp}, T]$ and 0 elsewhere is a rectangular pulse shaping filter. We transmit the OFDM signal at carrier frequency f_c . The transmitter is equipped with K antennas in a ULA with antenna spacing $c_0/2f_c$, where c_0 represents the speed of light. In this work, we assume a genie-aided beamformer to isolate the performance of the receiver. After beamforming with the beamforming function $\tilde{w}_a = e^{-j\pi a \sin \varphi}/2 + e^{-j\pi a \sin \theta}/2$, with φ being the angle of departure (AoD) of the tracked object, θ being the AoD of the communication receiver, and antenna index $a \in [0, K-1]$, the signal transmitted towards angle φ can be expressed as

$$\mathbf{s}_\varphi(t) = \sum_{a=0}^{K-1} \tilde{w}_a s(t) e^{j\pi a \sin \varphi}. \quad (1)$$

B. Channels

A part of the transmit signal is received by the UE while another part is reflected by the object of interest and reaches the sensing receiver co-located with the transmitter. The sensing channel is assumed to have one reflection caused by the tracked object with delay τ_o ,¹ associated Doppler shift

¹We do not distinguish between random variables and scalars notation-wise to maintain readability

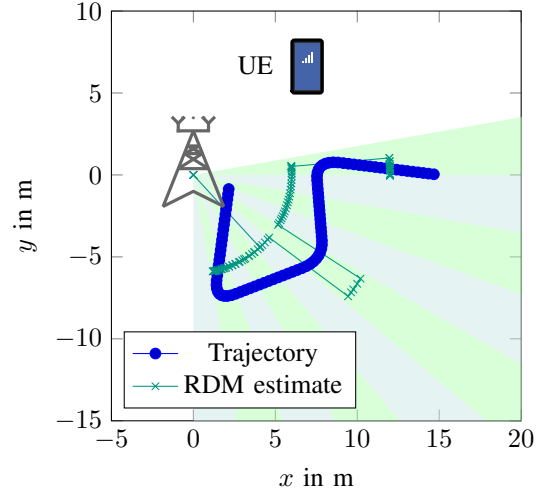


Fig. 1. Scenario: An example trajectory of a passive object is shown with the corresponding position estimate using the native RDM. The resolution of the RDM is not able to accurately capture the object trajectory.

$f_{D,o}$ and factor $a_o = 1$ representing the radar cross section, path loss and directivity gains. The received signal is given by

$$r(t) = a_o s(t - \tau_o) e^{j2\pi f_{D,o} t}.$$

Finally the signal $r(t)$ is normalized to the power σ_s^2 and then received by the different antennas, resulting in

$$\mathbf{r}_{\varphi,a}(t) = r(t) e^{j\pi a \sin \varphi} + q(t), \quad (2)$$

with independent noise $q(t) \sim \mathcal{CN}(0, \sigma_{ns}^2)$ at each antenna.

C. Sensing Receiver

At the sensing receiver, we first estimate the angle φ_{est} using the Bartlett method due to its computational complexity advantage [8]. Then, we perform receive beamforming based on φ_{est} . The received signal that is considered for estimating the radial velocity and the range, with $w_a = e^{-j\pi a \sin \varphi_{est}}$, is

$$\mathbf{r}_{\varphi_{est}}(t) = \sum_{a=0}^{K-1} w_a(\varphi_{est}) \mathbf{r}_{\varphi,a} e^{j\pi a \sin \varphi}. \quad (3)$$

We can define the instantaneous signal-to-noise ratio (SNR) for AoA estimation to $\text{SNR}_\varphi = \sigma_s^2 / \sigma_{ns}^2$, with σ_s^2 representing the end-to-end received signal power.

For estimating range and velocity, we follow the OFDM sensing processing from [9], i.e., we remove the cyclic prefix and transform the received signal to the time-frequency domain. After matched filtering, we obtain the received symbol matrix \mathbf{R} and with the corresponding transmitted matrix \mathbf{X} , we can compute the element-wise ratio matrix $\mathbf{Y} = \mathbf{R} \oslash \mathbf{X}$, with \oslash denoting the Hadamard division. The range-Doppler matrix (RDM) is calculated as

$$\text{RDM} = \text{IFFT} \left\{ \text{FFT} \left\{ \mathbf{Y} \right\} \right\}_{N \downarrow, M \rightarrow}, \quad (4)$$

with $M \rightarrow$ denoting that the given operation is performed on each row of the input matrix and $N \downarrow$ denoting that the operation is performed on each column of the matrix.

We estimate the range and velocity as the values \hat{r} and \hat{v} corresponding to the element of the RDM with maximum power, since we assume that there is always one object present. This peak detection is used for all methods described in this work, a discussion of different detectors such as super-resolution methods is left for future work due to the difficulty in computing their exact computation complexity. In Fig. 1, an example trajectory and the resulting estimated positions are shown.

III. SENSING SIGNAL PROCESSING

An OFDM-based JCAS system performing sensing on the received frame, as described in [9], suffers from a limited resolution, as the native 2D grid of the OFDM frame allows distinguishing between bins of spacing

$$r_{\text{res}} = \frac{c_0}{2B}, \quad (5)$$

$$v_{\text{res}} = \frac{c_0}{2f_c M T_0}. \quad (6)$$

The complexity of computing the RDM can be inferred from the fast Fourier transform (FFT) complexity as $5NM \cdot \log_2(NM)$ floating point operations (FLOPs) [10, Table 2]. Signal estimation can be improved through interpolation methods, including ZP of the frame or applying CZTs, or by using time correlation in the positions and applying tracking algorithms. In this section, we will introduce these methods in detail.

A. Interpolation Methods

1) *Zero-padding (ZP)*: The application of ZP before applying the inverse fast Fourier transform (IFFT) and the FFT in the sensing processing (4) is equivalent to a sinc-interpolation of the RDM. Both the required memory for the transform result as well as the computational effort for calculating the interpolated RDM increase with the ZP amount. As we are mostly interested in improving the range estimation, we zero-pad the frame by adding rows to the input matrix resulting in a frame of dimensions $N_{\text{pad}} \times M$. After ZP, we need to calculate N_{pad} IFFT values from N nonzero entries per original column, while the complexity of the FFT per row doesn't change. Therefore, the total complexity can be approximated as $5MN_{\text{pad}} \log_2(N_{\text{pad}}) + 5NM \log_2(M)$ FLOPs.

2) *Chirp Z-transform (CZT)*: The CZT generalizes the FFT to frequency components beyond the unit circle [11] and has been used to improve estimation in radar [12]. In our application, we are interested in the zoom capabilities of the transform, i.e., we use it to analyze a smaller section of the RDM in more detail. In the initial estimate, we use the whole RDM as an observation window as we assume no knowledge of the initial position. In the subsequent steps, we use the last estimate as the center of the observation window. The CZT as well as its inverse can be calculated with a complexity of $75(2N \log_2(2N))$ FLOPs, assuming the number of output and input values is both N . Note that this is five times higher than the complexity reported for the CZT in [10, Table 2]. In [10], the CZT complexity

is based only on the complexity of the underlying FFTs. However, we observe that the costs of other operations such as exponentiation are also significant. The total resulting complexity is $75M(2N \log_2(2N)) + 5NM \log_2(M)$ FLOPs. The resulting transform to generate a zoomed in section is calculated using:

$$\text{RDM}_{\text{fine}} = \underset{[A_r, W_r, N] \downarrow}{\text{CZT}} \left\{ \underset{[A_v, W_v, M] \rightarrow}{\text{CZT}} \{ \mathbf{Y} \}^* \right\}^*, \quad (7)$$

where the parameters are chosen as $W_r = e^{j2\pi r_{\text{CZT}}/(N^2 r_{\text{res}})}$, $A_r = e^{j2\pi(\frac{\hat{r}}{N r_{\text{res}}} - \frac{r_{\text{CZT}}}{2N r_{\text{res}}})}$, $W_v = e^{j2\pi/M}$ and $A_v = -1$, with the last range estimate \hat{r} as the center of the range observation window of size r_{CZT} . The range and velocity estimates corresponding to the element of RDM_{fine} with maximum power can then be obtained. These are more precise than estimation using the native RDM.

In our scenario, we use the CZT to increase the range estimation accuracy.

B. Tracking

1) *Kalman Filter*: The Kalman filter can be divided into two distinct phases: the prediction phase and the update phase. In the prediction phase, the filter uses the current estimate \mathbf{x}_{k-1} and the system dynamics \mathbf{F} to predict the range, velocity and angle at the next time step. With our model, the prediction equation of the Kalman filter at time step k is given by

$$\mathbf{x}_{k|k-1} = \begin{pmatrix} r_{k|k-1} \\ v_{k|k-1} \\ \varphi_{k|k-1} \end{pmatrix} = \underbrace{\begin{pmatrix} 1 & -T_0 & 0 \\ 0 & 1 & 0 \\ 0 & 0 & 1 \end{pmatrix}}_{\mathbf{F}} \cdot \mathbf{x}_{k-1}, \quad (8)$$

with \mathbf{x}_{k-1} denoting the output estimate of the Kalman filter in time step $k-1$ and $r_{k|k-1}$, $v_{k|k-1}$, $\varphi_{k|k-1}$ denoting the predicted range, radial velocity and AoA, respectively. As the radial velocity is defined to be positive for movements towards the receiver, we predict the new range as $r_{k|k-1} = r_{k-1} - T_0 v_{k-1}$. During the update phase, the filter incorporates new measurements to correct the predicted state, weighting the impact of the measurement with Kalman gain \mathbf{K} . By combining these two phases, the Kalman filter continuously refines its estimates, leading to an increased accuracy. The behavior of the system is influenced by the observation noise $\Sigma_{\text{meas},k}$, the noise caused by the resolution limit and the prediction noise $\Sigma_{\text{pred},k}$. The computational complexity of a Kalman filter is $\mathcal{O}_{\text{KF}}(s^3)$ with s denoting the size of the state space (which is 3 in our case).

2) *Event-Based Measurement (EBM)*: Seeking a low-complexity solution for accurate object tracking and recognizing that the RDM estimates \hat{r} and \hat{v} provide limited information, we propose an alternative range estimation method that combines linear prediction with event-based measurements:

$$r_{\text{ebm},k} = \begin{cases} \frac{1}{2}(\hat{r}_k + \hat{r}_{k-1}) & , \quad \hat{r}_k \neq \hat{r}_{k-1} \\ r_{\text{ebm},k-1} - T_0 \hat{v}_k & , \quad \hat{r}_k = \hat{r}_{k-1} \end{cases} \quad (9)$$

As the range resolution is low, we use the RDM range estimate \hat{r}_k if it changed compared to the last estimate \hat{r}_{k-1} and set the output to the mean of \hat{r}_k and \hat{r}_{k-1} . In all other cases, we rely on the linear prediction assuming a constant velocity of the target.

C. KalmanCZT

We propose the KalmanCZT approach that combines tracking and filtering with a Kalman filter and the interpolation capabilities of the CZT. We specifically address improving the range estimation of object tracking. A high-level block diagram of the KalmanCZT is shown in Fig. 2. As the Kalman filter estimates the covariance matrix $\Sigma_{\text{est},k|k-1}$ of the prediction, we use this estimate to determine the observation window of the CZT, as well as using the predicted value $\mathbf{x}_{k|k-1}$ as the center of the observation window of the CZT.

In Algorithm 1, the KalmanCZT estimator is detailed. We first perform the prediction given by (8), then feed the output values as the center of the observation window to the CZT. The covariance matrix $\Sigma_{\text{est},k|k-1}$ indicates the accuracy of the state estimates; therefore we use it to define the observation window of the CZT. As we want to ensure that the actual target range is in the observation window, we choose six times the standard deviation of the range as observation range r_{CZT} , using the three-sigma rule. We add a minimum range of 1 cm. We calculate the CZT parameters $W_{r,k}$ according to this choice and $A_{r,k}$ according to the predicted range-Doppler estimate $\mathbf{x}_{k|k-1}$. After applying the CZT, we extract the range measurement r_{est} and velocity measurement v_{est} corresponding to the delay-Doppler observation with maximum power and combine them into an estimation vector $\mathbf{z}_k = (r_{\text{est}} \ v_{\text{est}} \ \varphi_{\text{est}})^\top$. As we assume the measurement noise to be mostly attributed to the resolution $d_{\text{CZT},k} = r_{\text{CZT},k}/N_{\text{CZT},1}$, we model it as uniform noise, resulting in the updated range variance

$$\Sigma_{\text{meas}}[0,0] = \int_{-d_{\text{CZT},k}/2}^{d_{\text{CZT},k}/2} \frac{x^2}{d_{\text{CZT},k}} dx = \frac{d_{\text{CZT},k}^2}{12},$$

while the other components of Σ_{meas} are not updated. Finally, the Kalman gain \mathbf{K} is updated based on the covariance matrices and the regular update step of the Kalman filter is performed.

D. Performance Indicators

We use the Cramér-Rao bound (CRB) for benchmarking all sensing estimates. The CRB is a fundamental lower bound of the estimation error, but does not consider time dependence of the parameters to be estimated. In a tracking scenario, we may get an estimation accuracy below the CRB. For the AoA, the CRB can be formulated according to [13, Ch. 8.4] as

$$\text{Var}(\varphi_{\text{est}} - \varphi) = \frac{6\sigma_{\text{ns}}^2 (\sigma_{\text{ns}}^2 + K\sigma_s^2)}{\pi^2 \cos(\varphi)^2 N_{\text{win}} \sigma_s^4 K^2 (K^2 - 1)}. \quad (10)$$

Algorithm 1 KalmanCZT algorithm

Initialize state estimate $\mathbf{x}_{\text{track},0}$, covariance $\Sigma_{\text{est},0|0}$ and prediction noise Σ_{pred}
for each time step k **do**
 Prediction step:
 $\mathbf{x}_{k|k-1} = \mathbf{F} \mathbf{x}_{k-1}$
 $\Sigma_{\text{est},k|k-1} = \mathbf{F} \Sigma_{\text{est},k-1|k-1} \mathbf{F}^T + \Sigma_{\text{pred}}$
 CZT measurement:
 $r_{\text{CZT},k} = \max(6\sqrt{\Sigma_{\text{est},k|k-1}[0,0]}, 1 \text{ cm})$
 $d_{\text{CZT},k} = r_{\text{CZT},k}/N_{\text{CZT},1}$
 $W_{r,k} = e^{(j2\pi r_{\text{CZT},k}/(N_{\text{CZT},1} N_{r_{\text{res}}}))}$
 $A_{r,k} = e^{j2\pi \max\left\{0, \frac{\mathbf{x}_{k|k-1}[0]}{N_{r_{\text{res}}}} - \frac{r_{\text{CZT},k}}{2N_{r_{\text{res}}}}\right\}}$
 $\mathbf{Z}_k = \begin{bmatrix} \text{CZT} \\ [A_{r,k}, W_{r,k}, N_{\text{CZT},1}] \downarrow \end{bmatrix} \left\{ [A_v, W_v, N_{\text{CZT},2}] \rightarrow \{ \mathbf{R} \odot \mathbf{X} \}^* \right\}^*$
 $r_{\text{est}}, v_{\text{est}} = \text{Peak power detection}(\mathbf{Z}_k)$
 $\mathbf{z}_k = (r_{\text{est}}, v_{\text{est}}, \varphi_{\text{est}})^\top$
 $\Sigma_{\text{meas},k}[0,0] = \frac{d_{\text{CZT},k}^2}{12}$
 Update step:
 $\mathbf{K}_k = \Sigma_{\text{est},k|k-1} (\Sigma_{\text{est},k|k-1} + \Sigma_{\text{meas},k})^{-1}$
 $\mathbf{x}_k = \mathbf{x}_{k|k-1} + \mathbf{K}_k (\mathbf{z}_k - \mathbf{x}_{k|k-1})$
 $\Sigma_{\text{est},k|k} = (\mathbf{I} - \mathbf{K}_k) \Sigma_{\text{est},k|k-1}$
end for

We average over the full angle range using $\frac{1}{2\pi} \int_{-\pi}^{\pi} \cos(x)^2 dx = \frac{1}{2}$ to formulate an average CRB

$$\overline{\text{Var}}(\varphi_{\text{est}} - \varphi) = \frac{12\sigma_{\text{ns}}^2 (\sigma_{\text{ns}}^2 + K\sigma_s^2)}{\pi^2 N_{\text{win}} \sigma_s^4 K^2 (K^2 - 1)}. \quad (11)$$

For the range and velocity estimation bounds of the native RDM, we bound the error to the quantization noise introduced by the resolution limit instead of the CRB [14].

With the quantization introduced by the bins, the lower bounds are

$$\text{Var}(\hat{r} - r) \geq \frac{c_0^2}{12(2N_{\text{FFT}} \Delta f)^2} \quad \text{and} \quad (12)$$

$$\text{Var}(\hat{v}_{\text{rad}} - v_{\text{rad}}) \geq \frac{c_0^2}{12(2f_c M_{\text{FFT}} T_0)^2}. \quad (13)$$

IV. SIMULATION RESULTS

A. Parameters

We consider an OFDM system with carrier frequency $f_c = 5 \text{ GHz}$, a bandwidth of $B = 25 \text{ MHz}$, and $N = 2048$ subcarriers with a cyclic prefix length of $N_{\text{cp}} = 30$. All simulation scenarios assume a constant $\text{SNR}_\varphi = 0 \text{ dB}$, independent of range variation. We group $M = 259$ OFDM symbols in one frame for sensing. Therefore, the bounds (11)-(13) can be calculated as

$$\sqrt{\text{Var}(\varphi_{\text{est}} - \varphi)} = 6.8 \cdot 10^{-4} \text{ (rad)} \quad (14)$$

$$\sqrt{\text{Var}(\hat{r} - r)} = 1.73 \text{ (m)} \quad (15)$$

$$\sqrt{\text{Var}(\hat{v}_{\text{rad}} - v_{\text{rad}})} = 0.409 \text{ (m/s)}. \quad (16)$$

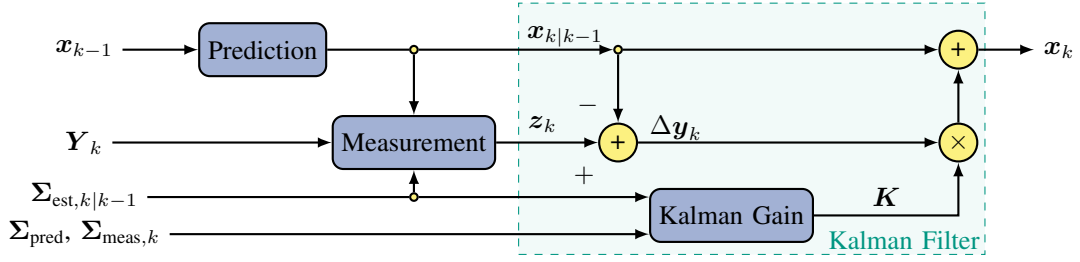


Fig. 2. Flowgraph of the proposed joint tracking and filtering algorithm KalmanCZT

With the native RDM resolution, the range is the most limiting factor to reconstruct the trajectory accurately while the AoA can be estimated quite accurately, as illustrated in Fig. 1.

B. Configuration of Interpolation Methods

We choose $N_{CZT} = 2048$ and use the complexity estimates in Tab. I to calculate the required FFT length $N_{\text{pad}} = 16N$ after ZP, such that ZP and the CZT have a similar complexity.

To get the same range resolution in the CZT as in the ZP, we configure the CZT in (7) as

$$A_v = -1, \quad W_v = e^{j2\pi/M}, \quad M = 259 \quad \text{and} \\ A_r = e^{j2\pi(\frac{\hat{r}_{\text{res}}}{N_{\text{res}}} - 2^{-5})}, \quad W_r = e^{j\pi 2^{-14}}, \quad N_{CZT} = 2^{11}.$$

C. Configuration of Tracking Algorithms

For the Kalman filter, the input values for the prediction and measurement covariance matrices significantly influence the behavior. Using experiments, we set them to

$$\Sigma_{\text{meas}} = \text{diag}(4.4 \quad 0.01 \quad 0.01)^\top, \quad \text{and} \\ \Sigma_{\text{pred}} = \text{diag}(1.3 \cdot 10^{-5} \quad 0.8 \quad 0.4)^\top, \quad (17)$$

with $\text{diag}(\cdot)$ denoting the diagonal matrix operator. We initialize $\Sigma_{\text{est}} = \mathbf{0}$ if the initial position is known exactly and $\Sigma_{\text{est}} = \text{diag}(r_{\text{res}} \quad v_{\text{res}} \quad \frac{1}{2})^\top$ when using the native RDM of the initial position is available. For the KalmanCZT, we choose the same initial Σ_{meas} , Σ_{est} , Σ_{pred} and prediction matrix F .

D. Complexity Discussion

We show a complexity estimate for each method in Tab. I. The RDM has the lowest complexity, and we chose the parameters of ZP and the CZT to have similar complexity. On the other hand, the memory requirement for ZP is 16 times the memory required for the other approaches. The tracking algorithms introduce minimal additional complexity of $C_K \approx 50$ FLOPs.

E. Performance Comparison

Assuming that the initial position is known exactly, as commonly assumed in the tracking literature, the RMSE of the estimates for 1000 trajectories consisting of 92 points is shown in Tab. II. In addition to the estimates, we show the mean Euclidean distance between estimated and true positions in the last column. The range and velocity error and of the RDM and ZP match the bounds of (12), while the AoA error

TABLE I
COMPLEXITY COMPARISON

Method	Complexity (FLOPs)
RDM	$C_0 = 5NM \log_2(NM)$
Kalman filter	$C_0 + C_K$
EBM	$C_0 + 3$
ZP	$5MN_{\text{pad}} \log_2(N_{\text{pad}}) + 5NM \log_2(M)$
CZT	$C_{CZT} = 75M(2N \log_2(2N)) + 5NM \log_2(M)$
KalmanCZT	$C_{CZT} + C_K$

TABLE II
ROOT MEAN SQUARED ERROR (RMSE) WITH KNOWN INITIAL POSITION

Method	range	velocity	AoA	position
RDM	1.715 m	0.40 m/s	0.08°	1.51 m
Kalman filter	0.156 m	0.40 m/s	0.08°	0.12 m
EBM	0.321 m	0.40 m/s	0.08°	0.24 m
ZP	0.109 m	0.40 m/s	0.08°	0.06 m
CZT	0.214 m	0.40 m/s	0.08°	0.12 m
KalmanCZT	0.003 m	0.41 m/s	0.08°	0.02 m

does not reach the CRB (11). This is expected behavior, since more intricate estimators such as super-resolution methods are needed to achieve performance close to CRB.

For the range error, we achieve the lowest error of 0.003 m with the KalmanCZT, followed by ZP with an RMSE of 0.11 m and Kalman filtering with an RMSE of 0.16 m. Notably, the EBM also significantly improves performance down to an RMSE of 0.32 m, while remaining the lowest complexity option.

We achieve a very similar performance for all velocity estimators. We have configured the CZT and ZP to result in the same velocity accuracy as the RDM. As the velocity can fall off quickly, tracking methods do not improve estimation and in the case of KalmanCZT even slightly worsen it. This is most probably due to mismatched Σ_{meas} and Σ_{pred} , and can be remedied by further tuning. Additional tracking does not seem to improve the AoA estimate either.

The position error is significantly reduced in all methods compared to the RDM estimate of 1.51 m, with the KalmanCZT resulting in the lowest error of 2 cm. A ZP approach of similar complexity reaches an error of 6 cm, while all other approaches also allow for a lower mean Euclidean distance in a range of 12-24 cm. We get the smallest improvement by employing the EBM.

In Fig. 3, we show the RMSE of the range estimate for

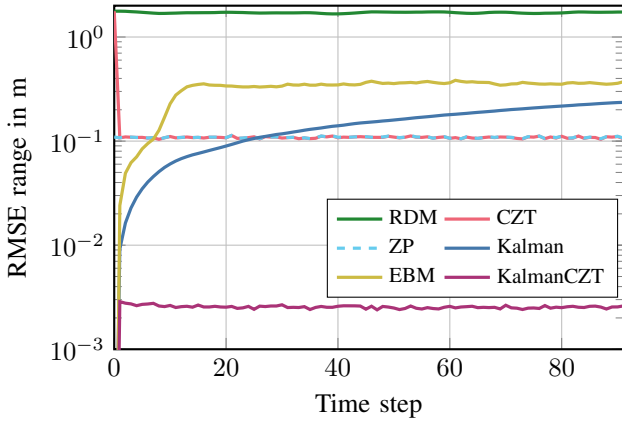


Fig. 3. Tracking accuracy over time RMSE vs. trajectory index with known start position

different estimation and tracking variants averaged over 1000 trajectories, under the assumption that the initial ground truth values are known. Therefore, the error in the first time step is zero for all algorithms with tracking component. The estimate based on the native RDM performs worst and does not change over time. The Kalman filter starts with an error of zero that gradually increases up to ≈ 0.25 m. The EBM starts with a behavior similar to the Kalman filter but reaches its stable error plateau after 15 samples and maintains an error of 0.33 m for the rest of the observation. The performance of CZT and ZP is identical, except for the first time step where the CZT performance equals the RDM estimate, as it needs initialization of its observation window. The difference in the first time step is the reason for the higher RMSE of CZT in Tab. II when compared to ZP. Lastly, leveraging not only a tracking mean but also a tracking variance in the KalmanCZT, the performance jumps from the initial estimate with an error of 0 to an error plateau of 2.5 mm.

Results for the case where the initial position is not fully known, but instead the initial RDM estimate is used for all initial tracking estimates, are shown in Fig. 4. For the Kalman filter and the EBM, we observe a decreasing error behavior from the initial RDM accuracy in contrast to Fig. 3. The EBM shows a consistent small gap to the performance of the Kalman filter. The KalmanCZT has the best performance, starting at a slightly higher error but very quickly decreasing to the same error floor as in Fig. 3.

V. CONCLUSION

In this paper, we provide an analysis on estimation accuracy enhancing methods with a focus on range estimation in OFDM-based JCAS systems. We compare tracking methods and interpolation methods and propose the KalmanCZT approach, that combines estimation based on the CZT with Kalman filtering. The range estimation error can be reduced from ≈ 1.7 m to ≈ 3 mm and the importance of tracking initialization is pointed out by comparing tracking with a known initial position and a known initial estimate. We provide a detailed complexity analysis, noting that the additional complexity for tracking algorithms is very low compared to the

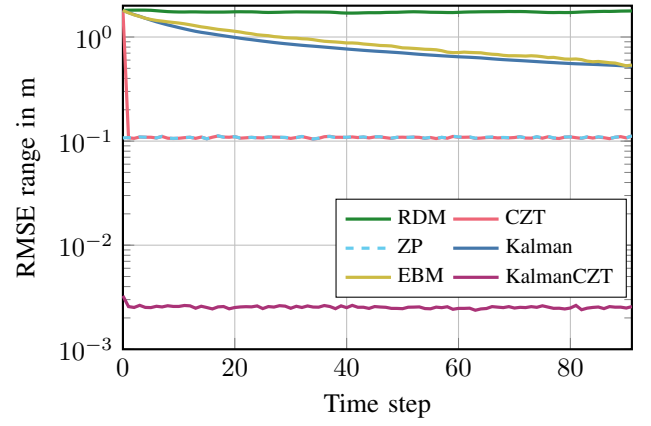


Fig. 4. Tracking accuracy over time RMSE vs. trajectory index with start position being the RDM estimate

computation of the RDM. Application of the CZT instead of the FFT yields improved estimation, for a controlled increase in computational complexity. The KalmanCZT approach provides a flexible estimation controlled by the dynamics of the tracked object, enabling efficient use of the computational resources.

For future investigations we are planning to extend the approach in order to apply it to real measurement data.

REFERENCES

- [1] T. Wild, V. Braun, and H. Viswanathan, "Joint design of communication and sensing for beyond 5G and 6G systems," *IEEE Access*, vol. 9, 2021.
- [2] M. Braun, C. Sturm, and F. K. Jondral, "Maximum likelihood speed and distance estimation for OFDM radar," in *Proc. IEEE Radar Conf.*, 2010.
- [3] Y. Xu, H. Yi, W. Zhang, and H. Xu, "An improved CZT algorithm for high-precision frequency estimation," *Applied Sciences*, vol. 13, no. 3, p. 1907, Feb. 2023.
- [4] Y. Liu, G. Liao, Y. Chen, J. Xu, and Y. Yin, "Super-resolution range and velocity estimations with OFDM integrated radar and communications waveform," *IEEE Trans. Veh. Technol.*, vol. 69, no. 10, Oct. 2020.
- [5] M. Lipka, E. Sippel, and M. Vossiek, "An extended Kalman filter for direct, real-time, phase-based high precision indoor localization," *IEEE Access*, vol. 7, 2019.
- [6] D. Burghal, N. A. Abbasi, and A. F. Molisch, "A machine learning solution for beam tracking in mmWave systems," in *Proc. Asilomar Conf. Signals, Systems, and Computers*, Nov. 2019.
- [7] J. B. Sanson, D. Castanheira, A. Gameiro, and P. P. Monteiro, "Co-operative method for distributed target tracking for OFDM radar with fusion of radar and communication information," *IEEE Sens. J.*, vol. 21, no. 14, Jul. 2021.
- [8] H. Obeidat, "Performance comparisons of angle of arrival detection techniques using ULA," *Wireless Personal Communications*, vol. 126, no. 4, pp. 3611–3623, 2022.
- [9] K. M. Braun, "OFDM radar algorithms in mobile communication networks," Ph.D. dissertation, Karlsruher Institut für Technologie (KIT), 2014.
- [10] S. Chimmangi, P. J. Prins, and S. Wahls, "Fast nonlinear Fourier transform algorithms using higher order exponential integrators," *IEEE Access*, vol. 7, pp. 145 161–145 176, 2019.
- [11] V. Sukhoy and A. Stoytchev, "Generalizing the inverse FFT off the unit circle," *Scientific Reports*, vol. 9, no. 1, Oct. 2019.
- [12] Z. Xu, S. Qi, and P. Zhang, "A coherent CZT-based algorithm for high-accuracy ranging with FMCW radar," *IEEE Trans. Instrum. Meas.*, vol. 72, 2023.
- [13] H. L. van Trees, *Optimum Array Processing: Part IV of Detection, Estimation, and Modulation Theory*. Wiley, 2002.
- [14] M. Braun, C. Sturm, and F. K. Jondral, "On the single-target accuracy of OFDM radar algorithms," in *Proc. International Symposium on Personal, Indoor and Mobile Radio Communications (PIMRC)*, 2011.